

Halogen Substitution in Zero-Dimensional Mixed Metal Halides toward Photoluminescence Modulation and Enhanced Quantum Yield

Mingze Li, Yawen Li, Maxim S. Molokeyev, Jing Zhao, Guangren Na, Lijun Zhang,* and Zhiguo Xia*

Zero-dimensional (0D) organic–inorganic hybrid metal halides have unprecedented degrees of freedom for structural tunability and photoluminescence modulation. Here, the 0D isomorphous hybrid metal mixed halides $(\text{C}_9\text{NH}_{20})_9\text{Pb}_3\text{Zn}_2\text{Br}_{19(1-x)}\text{Cl}_{19x}$ ($x = 0-1$) with continuous halogen contents control, exhibiting tunable emission and enhancement of photoluminescence quantum yield (PLQY) are reported. The competitive bromine to chlorine substitution process in $(\text{C}_9\text{NH}_{20})_9\text{Pb}_3\text{Zn}_2\text{Br}_{19(1-x)}\text{Cl}_{19x}$ occurs first in $[\text{ZnBr}_{4-x}\text{Cl}_x]^{2-}$ tetrahedron before the $[\text{Pb}_3\text{Br}_{11-x}\text{Cl}_x]^{5-}$ trimer. The increasing Cl content in samples from $x = 0$ to 1 results in an expected blue shift of emission peak from 565 to 516 nm, and meanwhile a strikingly room temperature PL quantum yield increase from 8% to 91%. Combined experimental characterizations and theoretical calculations indicate that the blue shift of interband transition energy is responsible for the emission peak shift. Moreover, with the increasing Cl content, the enhanced electron–phonon interaction and the weakened thermal-assisted nonradiative recombination result in more efficient radiative transition channels and ultimately enhanced PLQY. The impact of halogen substitution on electronic structures and optical properties in 0D hybrid metal halides is emphasized in this work as a new strategy to promote the future development of new luminescent materials.

in photodetectors,^[1] white-light emitting diodes (WLEDs),^[2] X-ray scintillations,^[3] luminescent sensors,^[4] etc. It is noteworthy that 0D here is defined as the molecular level concept, in which the non-networked individual metal halide units or clusters act as a judging criteria for this type of materials. Generally, selecting large organic ligands and single inorganic component to build a 0D framework is a simple design principle. Accordingly, many metal halides have been synthesized and show broadband emissions attributed to the self-trapped excitons (STEs).^[3,5] However, the spectral adjustment of such materials remains a challenge due to the nonadjustable STEs emission, which greatly restrict their further applications. In addition, photoluminescence quantum yield (PLQY) at room temperature (RT) is regarded as one of the key points for evaluating the performance of such luminescent materials. Some recent researches have reported 0D metal halides with ultra-high PLQYs at RT,^[5c,5d] and despite similar 0D structures, the values reported in other work are much lower.^[5a,6] To understand


this unusual phenomenon, further experimental investigation and mechanism explanation are necessary, by which it will provide directions for comprehending the luminescence mechanism of 0D family and further exploring other new materials with high PLQY.

1. Introduction

Zero-dimensional (0D) organic–inorganic hybrid metal halides belong to a class of emerging optoelectronic materials with unique host–guest structures, suggesting large potentials

M. Z. Li, Prof. J. Zhao, Prof. Z. G. Xia
The Beijing Municipal Key Laboratory of New Energy Materials and Technologies
School of Materials Sciences and Engineering
University of Science and Technology Beijing
Beijing 100083, P. R. China
E-mail: xiazg@scut.edu.cn; xiazg@ustb.edu.cn

Y. W. Li, G. R. Na, Prof. L. J. Zhang
State Key Laboratory of Integrated Optoelectronics
Key Laboratory of Automobile Materials of MOE
College of Materials Science and Engineering
Jilin University
Changchun 130012, China
E-mail: lijun_zhang@jlu.edu.cn

 The ORCID identification number(s) for the author(s) of this article can be found under <https://doi.org/10.1002/adom.202000418>.

Prof. M. S. Molokeyev
Laboratory of Crystal Physics
Kirensky Institute of Physics
Federal Research Center KSC SB RAS
Krasnoyarsk 660036, Russia

Prof. M. S. Molokeyev
Siberian Federal University
Krasnoyarsk 660041, Russia

Prof. M. S. Molokeyev
Department of Physics
Far Eastern State Transport University
Khabarovsk 680021, Russia

Prof. Z. G. Xia
State Key Laboratory of Luminescent Materials and Devices
Institute of Optical Communication Materials
South China University of Technology
Guangzhou 510641, China

DOI: 10.1002/adom.202000418

Halogen substitution is a widely used strategy to adjust luminescence properties of different metal halides.^[7] Recent studies have revealed the effects of halogens on the optical properties of two-dimensional (2D) hybrid metal halides, in which the distinct trapping and de-trapping energies from different halogens will significantly affect the STEs emissions, and Br-based compounds always show highest PLQY that can be ascribed to the thermal equilibrium between the free excitons and STEs.^[8] However, the situation could be quite different due to the different crystal structures and electronic structures in 0D materials. The highly localized excitons in 0D molecular species indicate that there are no free excitons in 0D systems, in that case the optical properties are mainly ascribed to the STEs of isolated inorganic units. Thus, there remains a challenge to understand the relationships between the halogen substitution and luminescence properties in 0D metal halides.

Here, we first obtained $(\text{C}_9\text{NH}_{20})_9[\text{Pb}_3\text{Br}_{11}](\text{ZnBr}_4)_2$ with trigonal space group $P31c$, and further prepared the isostructural solid solutions of 0D mixed halogen hybrid metal halides, $(\text{C}_9\text{NH}_{20})_9\text{Pb}_3\text{Zn}_2\text{Br}_{19(1-x)}\text{Cl}_{19x}$ ($x = 0-1$), in which two distinct inorganic building units are isolated by large organic ligand 1-buty-1-methylpyrrolidinium $(\text{C}_9\text{NH}_{20})^+$. $(\text{C}_9\text{NH}_{20})_9[\text{Pb}_3\text{Br}_{11}](\text{ZnBr}_4)_2$ exhibits broadband yellow emission peaking at 565 nm, but suffers from low PLQY at RT. By introducing Cl^- in this chemical system, we achieved significant blue shift of the emission along with remarkable improvement of the PLQY with the Cl-based end-member reaching 91% PLQY at RT. Based on joint experiment–theory characterization, the enhancement of PLQY with the increasing Cl content is attributed to the enhanced electron–phonon (e - p) interaction and weakened thermal-assisted nonradiative recombination. Our work not only reveals the

important role of halogen substitution in the structural adjustment in 0D organic–inorganic hybrid metal halides, but also provides promising guidance to achieve luminescence modulation and emission efficiency improvement based on these materials.

2. Results and Discussion

Single crystals of $(\text{C}_9\text{NH}_{20})_9\text{Pb}_3\text{Zn}_2\text{Br}_{19(1-x)}\text{Cl}_{19x}$ ($x = 0-1$) were grown by a simple solution method as described in the Experimental Section. The single crystal X-ray diffraction was used to solve the crystal structures, and the trigonal space group $P31c$ was determined in this system. It is worth mentioning that a similar 0D metal halide with same formula, but albeit with different space group, had been published recently.^[5d] In order to make a comparison between our structural model ($P31c$) with previously obtained model ($P6_3$) for $(\text{C}_9\text{NH}_{20})_9[\text{Pb}_3\text{Cl}_{11}](\text{ZnCl}_4)_2$, first we decided to check $P6_3$ for consistency. Careful checking of $P6_3$ structure revealed that H...H contacts between close $(\text{C}_9\text{NH}_{20})^+$ molecules in $(\text{C}_9\text{NH}_{20})_9[\text{Pb}_3\text{Cl}_{11}](\text{ZnCl}_4)_2$ are located at very close distances: 0.74, 1.25 Å, etc., and the two molecules C_9NH_{20} are overlapped, which can happen only in the case of structural disorder. In our model there are no collisions of molecules and all molecules are located at good distances from each other. Therefore, we can suggest that $P31c$ group is valid for this compound and $(\text{C}_9\text{NH}_{20})_9[\text{Pb}_3\text{Cl}_{11}](\text{ZnCl}_4)_2$ structure can be refined once again using the new space group. As the basic compound, $(\text{C}_9\text{NH}_{20})_9[\text{Pb}_3\text{Br}_{11}](\text{ZnBr}_4)_2$ shows a typical 0D structure with the isolated anionic lead-halide octahedral trimer, $[\text{Pb}_3\text{Br}_{11}]^{5-}$ and tetrahedral $[\text{ZnBr}_4]^{2-}$, surrounded by

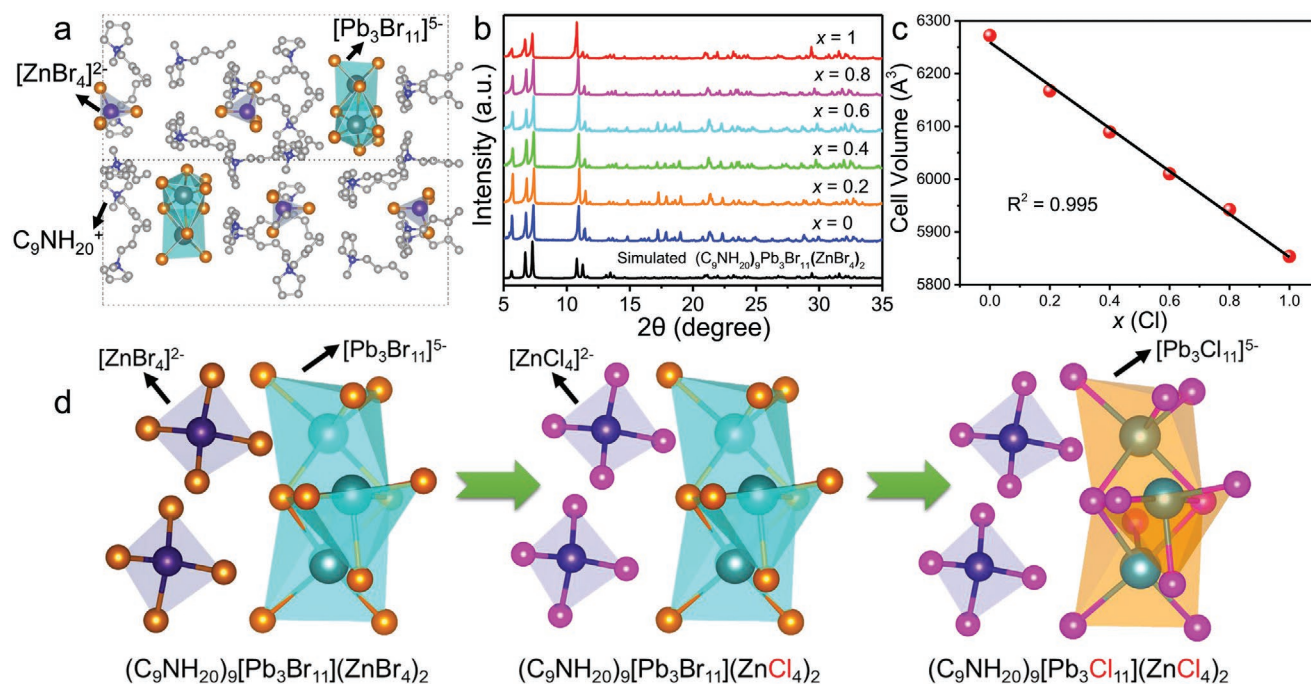


Figure 1. a) The unit-cell of the $(\text{C}_9\text{NH}_{20})_9[\text{Pb}_3\text{Br}_{11}](\text{ZnBr}_4)_2$ showing the two different polyhedrons, H atoms are omitted for clarity. b) The simulated and experimental X-ray powder patterns of $(\text{C}_9\text{NH}_{20})_9\text{Pb}_3\text{Zn}_2\text{Br}_{19(1-x)}\text{Cl}_{19x}$ ($x = 0, 0.2, 0.4, 0.6, 0.8$, and 1 , respectively). c) Unit cell volume V of $(\text{C}_9\text{NH}_{20})_9\text{Pb}_3\text{Zn}_2\text{Br}_{19(1-x)}\text{Cl}_{19x}$ samples as a function of x . d) The schematic diagram of the evolution process from $(\text{C}_9\text{NH}_{20})_9[\text{Pb}_3\text{Br}_{11}](\text{ZnBr}_4)_2$ to $(\text{C}_9\text{NH}_{20})_9[\text{Pb}_3\text{Cl}_{11}](\text{ZnCl}_4)_2$.

the large organic molecule $(C_9NH_{20})^+$ (Figure 1a). Moreover, by introducing Cl^- in the system, a series mixed halide compounds and Cl-based end-member compound was finally obtained. Figure 1b shows powder X-ray diffraction (XRD) of $(C_9NH_{20})_9Pb_3Zn_2Br_{19(1-x)}Cl_{19x}$ ($x = 0, 0.2, 0.4, 0.6, 0.8,$ and $1,$ respectively), the consistency of the simulated and experimental patterns indicates the isomorphism and high purity of all compounds. In addition, we provided difference plot of one selected compound ($x = 0.2$) and marked indexes of diffraction peaks (Figure S1, Supporting Information). One can see that actually all peaks were ideally fitted by unit cell and difference plot is smooth. We also provided the crystallographic information files (CIFs) of two end-member compounds in the Supporting Information. As shown in Figure S2 (Supporting Information), the bond length of three Pb and the Br at the top (Pb–Br1) and bottom (Pb–Br2) of trimer are 3.199 and 3.135 Å, which is larger than 3.056 and 2.976 Å for the bond length of Pb and the Cl at top (Pb–Cl1) and bottom (Pb–Cl2) of trimer. The main parameters of two compound are provided in the Table S1 (Supporting Information). As seen in Figure 1c, when proportion of Cl increased, the cell volume decreased due to the smaller radius of Cl and shorter bond length of Pb–Cl, and the well-fitted linear declining trend also indicate that the molecular formulas determined by the experimental design are very close to the actual situation. Simultaneously, the Cl/Br ratio was fixed in starting reagents and Le Bail profile fitting (Figure S3 and Table S2, Supporting Information) shows absence of impurity peaks, therefore all starting reagents were reacted and final compounds should have the same Cl/Br ratio. In addition, thermogravimetric analysis (TGA) demonstrate the high chemical stability (≈ 250 °C) of such materials (Figure S4, Supporting Information).

Although the XRD results confirmed the successful halogen substitution, the specific replacement process should be further studied since there are two halogen positions in different chemical environments. The calculated formation energy (see in Table 1) for $[ZnBr_{3.5}Cl_{0.5}]^{2-}$ and $[Pb_3Br_{10.5}Cl_{0.5}]^{5-}$ shows that the formation energy for Br substituted by Cl in $[ZnBr_4]^{2-}$ is larger than that of $[Pb_3Br_{11}]^{5-}$, and thus, we can conclude that the competitive process of halogen replacement will take place mainly in the $[Zn(Br/Cl)_4]^{2-}$ tetrahedron at first and then occurs in the $[Pb_3(Br/Cl)_{11}]^{5-}$ trimer (Figure 1d).

Table 1. Band gap, total energy (E_{total}), and formation energy (E_{form}) of $(C_9NH_{20})_{18}(Pb_3Br_{11})_2(ZnBr_4)_4$, $(C_9NH_{20})_{18}(Pb_3Br_{11})_2(ZnBr_4)_3(ZnCl)$, $(C_9NH_{20})_{18}(Pb_3Br_{11})(Pb_3Br_{10}Cl)(ZnBr_4)_4$, $(C_9NH_{20})_{18}(Pb_3Cl_{11})_2(ZnCl_4)_4$, $ZnBr_2$, $ZnCl_2$, $PbBr_2$, and $PbCl_2$.

Compounds	Band gap [eV]	E_{total} [eV]	E_{form} [eV atom ⁻¹]
$(C_9NH_{20})_{18}(Pb_3Br_{11})_2(ZnBr_4)_4$	3.603	−3076.28	—
$(C_9NH_{20})_{18}(Pb_3Br_{11})_2(ZnBr_4)_3(ZnCl)$	3.694	−3077.14	−0.308
$(C_9NH_{20})_{18}(Pb_3Br_{11})(Pb_3Br_{10}Cl)(ZnBr_4)_4$	3.691	−3077.04	−0.207
$(C_9NH_{20})_{18}(Pb_3Cl_{11})_2(ZnCl_4)_4$	3.627	−3095.90	—
$ZnBr_2$	—	−7.28577	—
$ZnCl_2$	—	−8.40127	—
$PbBr_2$	—	−9.65282	—
$PbCl_2$	—	−10.7641	—

Photographs of title compounds are shown in Figure 2a, and all large size (≈ 5 mm) crystals are colorless. Interestingly, one can clearly observe the tunable yellow to green emission under UV-light, attributed to the halogen replacement. To further reveal the effect of Br/Cl replacement on PL process, detailed investigations of optical properties are discussed below. Figure 2b displays the PLE and PL spectra of $(C_9NH_{20})_9Pb_3Zn_2Br_{19(1-x)}Cl_{19x}$, and all of the title compounds show broadband yellow/green emission with large Stokes shift. All the PL characteristics are consistent with typical characters of STEs emission which will be discussed below in detail. When the content of Cl increased, both the excitation peak and the emission peak show a significant blue shift, and the PLQY measured at RT also show an interesting improvement from 8% to 91% (Figure 2c). Simultaneously, PL decay time provided in Figure 3a was used to further understand the PL mechanism, and the lifetime can be all ideally fitted by a single exponential Equation (1): $I(t) = A \exp(-t/\tau)$. The calculated lifetimes show an increasing trend from $x = 0$ to 1, and the specific values are also described in Figure 3a. The different sensitivities of the thermal-assisted de-trapping pathway can well explain the variable lifetime. The monitored emission ranges from yellow with Commission Internationale de l'Eclairage (CIE) chromaticity coordinate of (0.405, 0.569) for Br-based sample to green (0.178, 0.599) for Cl-based sample (Figure 3b). Furthermore, the Cl-based sample maintained a high PLQY of 81.2% after half a year of exposure to the air, which indicates the high ambient stability of this type materials. In Table 2, we summarized the main optical parameters including the value of PLQY, full-width at half-maximum (FWHM), Stokes shift, lifetime, and CIE values. Thus, the optical analyses indicate that when Cl ions gradually replace Br ions, a blue shift of PL spectrum along with a substantial increase of PLQY is observed. Such phenomenon will undoubtedly bring guidance to the spectral adjustment and efficiency improvement of OD metal halide hybrids. However, the existing information is not sufficient to explain the causes of the above phenomenon, and thus further analysis is needed.

The spectra shift is undoubtedly due to the blue shift of interband transition energy, in which the excited states with higher energy of Cl-based halides will cause higher energy emissions.^[8] Figure S5 (Supporting Information) depicts UV–Vis reflectance spectra and the Tauc plot (insert of Figure S5, Supporting Information) showing the characteristics of the optical band gap. The band gaps become larger as Cl^- gradually replaces Br^- , which is very consistent with the blue shift of PL spectra. Moreover, density functional theory (DFT) calculations are also used to further study the electronic structure properties. Figure 4a and Figure S6 (Supporting Information) show the electronic structure and project density of states (PDOS) of $(C_9NH_{20})_9(Pb_3Br_{11})(ZnBr_4)_2$ and $(C_9NH_{20})_9(Pb_3Cl_{11})(ZnCl_4)_2$, respectively. Both the two compounds belong to direct band gap semiconductor with $E_g = 3.603$ and 3.625 eV at Γ (0.0, 0.0, 0.0). Consistent with the experimental trend, the Cl-based

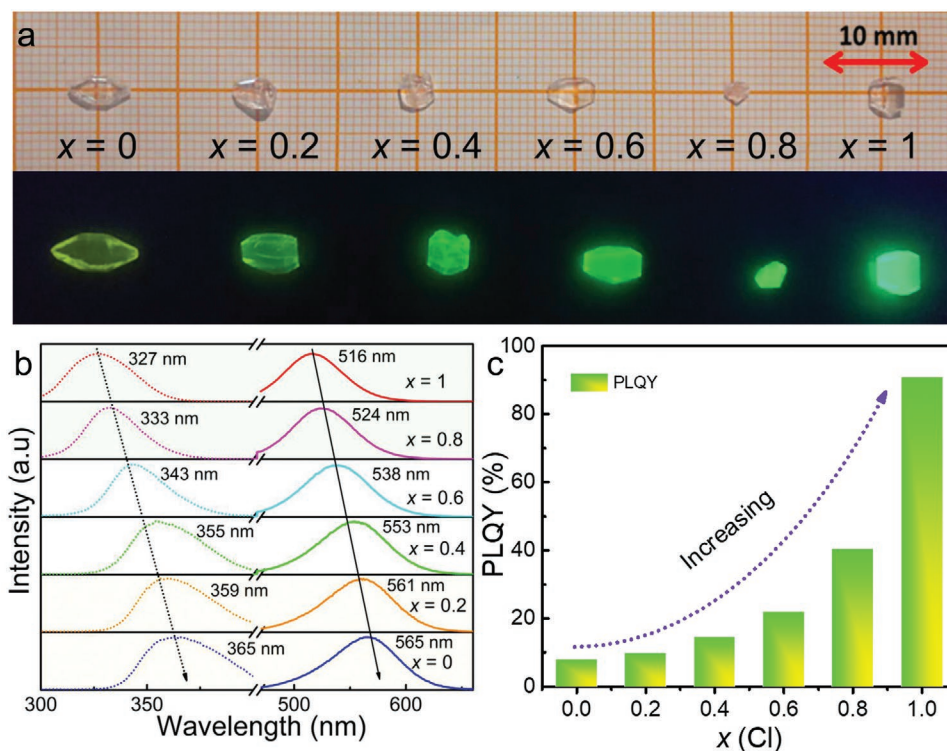


Figure 2. a) Optical photographs of as-grown $(\text{C}_9\text{NH}_{20})_9\text{Pb}_3\text{Zn}_2\text{Br}_{19(1-x)}\text{Cl}_{19x}$ ($x = 0, 0.2, 0.4, 0.6, 0.8,$ and $1,$ respectively) crystals under daylight (upper) and UV light (under). b) Room-temperature photoluminescence (PL; solid line) and photoluminescence excitation (PLE) spectra (dotted line) of $(\text{C}_9\text{NH}_{20})_9\text{Pb}_3\text{Zn}_2\text{Br}_{19(1-x)}\text{Cl}_{19x}$ monitored at corresponding optimum wavelengths. c) Variations of the PLQY of $(\text{C}_9\text{NH}_{20})_9\text{Pb}_3\text{Zn}_2\text{Br}_{19(1-x)}\text{Cl}_{19x}$ crystals with different excitation wavelength (365, 359, 355, 343, 333, and 327 nm, respectively).

structure has a larger band gap than Br-based structure. This difference provides theoretical basis for the transformation of the luminescent from yellow of Br-rich compounds to green of Cl-rich compounds. The PDOS and charge density distribution in valence band maximum (VBM) demonstrated that VBM of Br-based compound composed of Br-4p and Pb-6s states and the VBM of Cl-based compound composed of Cl-4p and Pb-6s compounds. The lower two-fold degenerate conduction band at ≈ 3.60 eV composed of organic cations and the higher conduction band at ≈ 4.12 eV derived from Pb-6p states. In addition, the $[\text{Zn}(\text{Br}/\text{Cl})_4]^{2-}$ clusters have no contribution to band edges, which indicate that the luminescence center in this system is ascribed to $[\text{Pb}_3(\text{Br}/\text{Cl})_{11}]^{5-}$ rather than $[\text{Zn}(\text{Br}/\text{Cl})_4]^{2-}$ clusters. The negligible dispersion of valence bands and conduction bands indicated scarcely electronic coupling due to long distance between trimer-trimer distances. The band structures

and PDOS for mixed halide compounds were also presented in Figure S7 (Supporting Information). Upon light excites, the excited electron transition from Pb-6s to Pb-6p_z orbital (shown in Figure 4b and Figure S4, Supporting Information), then the Coulomb repulsion between the excited electron in Pb-6p_z and Br-p pushes the Br1(Cl1) and Br2(Cl2) farther, resulting in structural relaxation and hence a large Stokes shift.

The effect of phonons is an important factor in STEs process, which can play the dual role of stimulating emission and suppressing emission.^[9] The strong e-p coupling will bring about excited state structural distortions, which is the cause of STEs. On the other hand, the phonon absorption-induced nonradiative recombination will significantly quench the STEs emission at high temperature. Therefore, a clear study of the effect of phonons in this system will hopefully explain the abnormal enhancement of PLQY.

The electronic properties of distorted Br-based and Cl-based structures at excited states were calculated to explore the possible effect of e-p interactions. We analyzed the band gap change as the function of the distortion as shown in Figure 5a. In these distorted structures, the halogen atoms shared by three octahedrons are moved up and down along c-direction, that is, bond lengths of Pb-X (X = Br, Cl) in Pb-trimer are elongated and shortened, as shown in Figure S1 (Supporting Information). As one can see, when the bond lengths of Pb-X1 (X = Br1, Cl1) and

Table 2. Summary of optical properties of $(\text{C}_9\text{NH}_{20})_9\text{Pb}_3\text{Zn}_2\text{Br}_{19(1-x)}\text{Cl}_{19x}$ ($x = 0, 0.2, 0.4, 0.6, 0.8,$ and $1,$ respectively).

x	PLQY [%]	FWHM [nm]	Stokes shift [nm]	Life time [ns]	CIE [x,y]
0	8.1	69	200	41.96	(0.405,0.549)
0.2	9.9	70	202	48.84	(0.381,0.566)
0.4	14.7	71	198	55.23	(0.357,0.581)
0.6	22.0	68	195	113.69	(0.285,0.609)
0.8	40.5	65	191	317.06	(0.221,0.611)
1	90.8	61	189	569.26	(0.178,0.599)

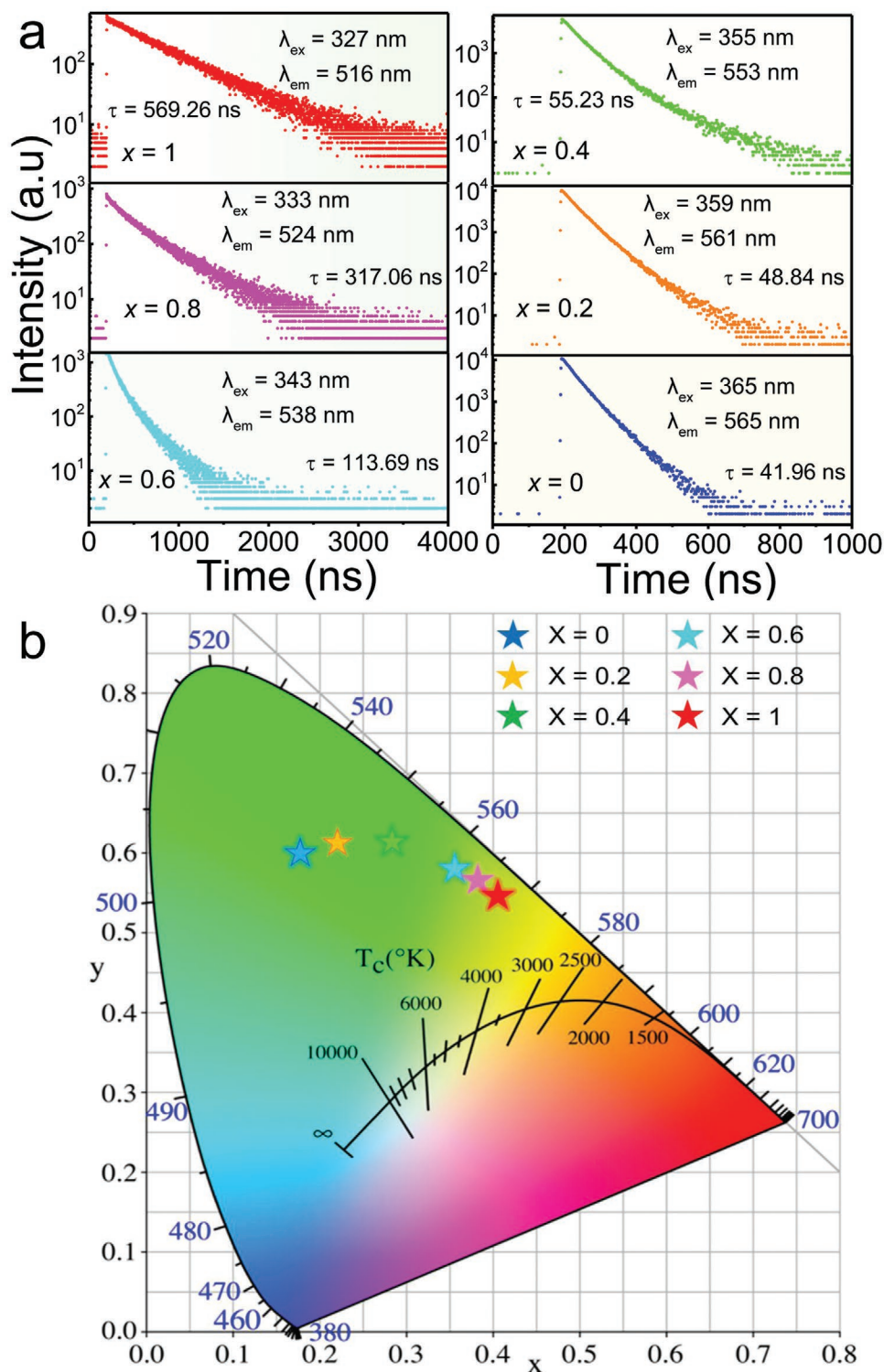


Figure 3. a) Room-temperature photoluminescence (PL) decay curves of $(C_9NH_{20})_9Pb_3Zn_2Br_{19(1-x)}Cl_{19x}$ ($x = 0, 0.2, 0.4, 0.6, 0.8,$ and $1,$ respectively). b) Commission Internationale de l'Eclairage (CIE) chromaticity diagram of $(C_9NH_{20})_9Pb_3Zn_2Br_{19(1-x)}Cl_{19x}$ crystals.

Pb-X2 ($X = Br, Cl$) are changed by the same magnitude, the band gap of Br-based and Cl-based compounds are decreased differently. But in general, the band gap of all-Cl compound changed more than that of Cl-based end-member compound.

The discrepancy in the sensitivity of band gap to structure is due to the difference in bond lengths. When the bond lengths of Pb-Br and Pb-Cl change by the same length, the relatively shorter bond length of the later means larger distortion. Since

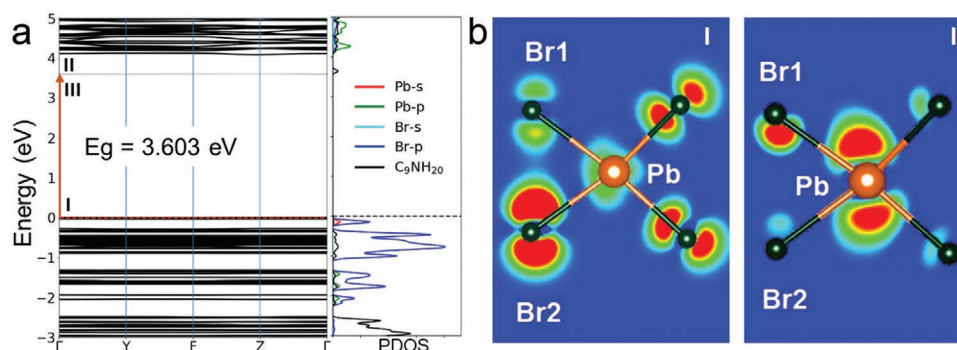


Figure 4. a) The calculated band structure (left) and the partial density of state (PDOS) (right) of $(\text{C}_9\text{NH}_{20})_9[\text{Pb}_3\text{Br}_{11}](\text{ZnBr}_4)_2$. b) The charge density at the valence band maximum (VBM) and the conduction band minimum of $(\text{C}_9\text{NH}_{20})_9[\text{Pb}_3\text{Br}_{11}](\text{ZnBr}_4)_2$. Isosurface value of charge density is set at $0.005e \text{ \AA}^{-3}$.

the VBM of two end-member are mainly composed by Pb-5s-X-4p (X = Cl/Br) antibonding states, the bond length of Pb-X is crucial to the position of VBM. Thus, the VBM position of Cl-based compound is more affected than that of the Br-based compound. As a result, when Pb-Cl bond length changes, the bonding strength of Pb-Cl become stronger or weaker and then the VBM elevated or suppressed more apparently.

Typical thermal-assisted de-trapping pathway was used to explain temperature-dependent quenching phenomenon, in which the phonon absorption restores the distorted lattice to its original state by nonradiative combinations at high temper-

ature.^[10] The radiative decay rate will be significantly reduced due to the competition with nonradiative pathway, and relatively low PLQY is thus obtained. However, no systematic research discussed the influence of halogen ions on this process, which may also have an impact due to the structural changes. Based on it, we proposed that one of the possible reasons for PLQY improvement was ascribed to the relatively hard lattice of Cl-based structure which can inhibit the temperature-dependent phonons absorption. Temperature-dependent PL spectra of all Br-based samples and all Cl-based samples from 200 to 380 K (Figure S8, Supporting Information) were measured to verify

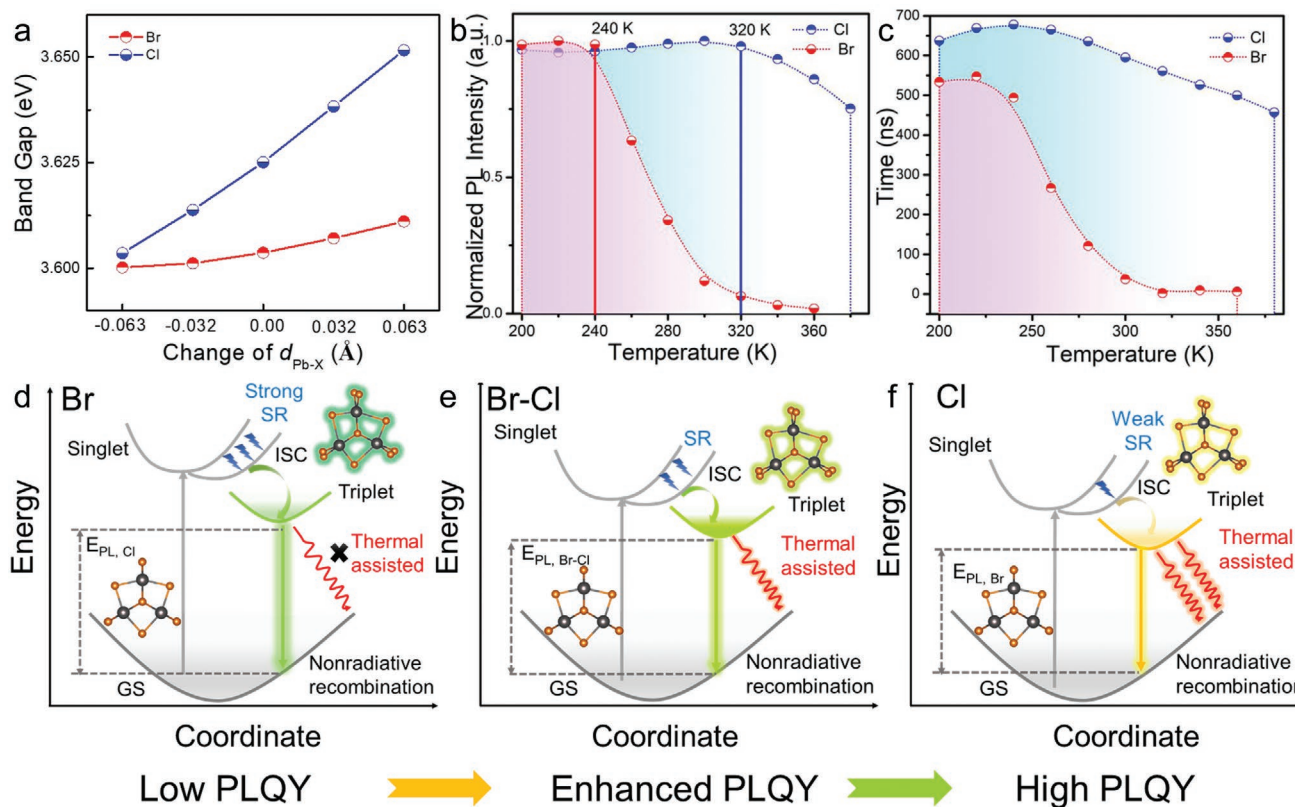


Figure 5. a) The change rate of band gap for distorted all-Br and all-Cl structures. b) Temperature-dependent normalized photoluminescence (PL) intensity from 200 to 380 K of $(\text{C}_9\text{NH}_{20})_9[\text{Pb}_3\text{Br}_{11}](\text{ZnBr}_4)_2$ and $(\text{C}_9\text{NH}_{20})_9[\text{Pb}_3\text{Cl}_{11}](\text{ZnCl}_4)_2$. c) Temperature-dependent PL decay time from 200 to 380 K of $(\text{C}_9\text{NH}_{20})_9[\text{Pb}_3\text{Br}_{11}](\text{ZnBr}_4)_2$ and $(\text{C}_9\text{NH}_{20})_9[\text{Pb}_3\text{Cl}_{11}](\text{ZnCl}_4)_2$. Schematic diagram of luminescence processes in d) all-Br based compound, e) mixed Br-Cl based compound, and f) all-Cl based compound, respectively. SR, structural reorganization; E_{PL} , emission energy.

our hypothesis, and temperature-dependent normalized PL intensity depicted in Figure 5b provides a comparison between the two end-member compounds. The temperature-dependent higher broadening of Br-based sample can be attributed to the softer phonons compared with Cl-based sample. As the results shown, Br-based sample has a much lower quenching temperature at about 240 K compared to the 320 K of Cl-based sample, in that case low PLQY of Br-based sample is not surprising. Moreover, the activation energy (E_a) of Br-based sample and Cl-based sample can be calculated by the following equation:

$$I(T) = \frac{I_0}{1 + A \exp\left(\frac{-E_a}{k_B T}\right)} \quad (1)$$

where $I(T)$ is the integrated PL intensity at specific temperature T (I_0 is the value at 0 K), and k_B is the Boltzmann constant. The results (Figure S9, Supporting Information) show that Cl-based sample have much higher E_a (523.34 meV) than the Br-based sample (304.13 meV), which also show more efficient radiative recombination channel in Cl-based samples. Another powerful evidence of the thermal-assisted de-trapping pathway is the variable lifetime value depending on temperature (Figure 5c),^[11] and specific decay curves are also provided in Figure S10 (Supporting Information). The intensive thermal drive acceleration of the PL lifetime occurs in all Br-based sample, while the process of Cl-based sample is much slower.

Based on the above results, we can conclude that there are two factors resulting in PLQY enhancement. First, the electronic properties of Cl-based compound are more sensitive to geometry structures, indicating strong electron–phonon interaction in Cl-based compound. Second, the relative soft Br-based lattice is easier effect by temperature and absorb phonons and then following nonradiative recombination. In contrast, the harder all-Cl lattice influenced weakly by temperature to maintain radiative recombination under high temperature.

As mentioned before, the broadband emission along with large Stokes Shifts belongs to the typical STEs emission. Singlet and triplet STEs emission have been widely studied for ns^2 metal halides,^[12] and heavy atom (Pb^{2+} , Bi^{3+}) effects lead to intersystem crossing (ISC) from singlet to triplet.^[13] Moreover, other evidences also supported this viewpoint as discussed below. Figure S11 (Supporting Information) shows the emission intensities at 565 and 516 nm excited at 375 nm as a function of the excitation power density of Br-based sample and Cl-based sample, respectively. Linear increasing trend in emission intensity exclude the effect of permanent defects which may also cause broadband emissions in OD system.^[5a] Furthermore, fs-transient absorption (fs-TA) spectrum provided in Figure S12 (Supporting Information) was used to monitor a direct signal in Br-based sample. Unlike the bleaching signal of permanent defects,^[9a,14] the mentioned compound exhibits broadband absorption upon 367 nm excitation. In addition, the formation time (≈ 200 fs) of STEs can also be determined by observing the rise time of the induced absorption (Figure S13, Supporting Information). Based on the discussion given above, we propose ration models as illustrated in Figure 5d–f. Under UV excitations, the electrons will be excited to the singlet state, the excited structure of $[Pb_3Br/Cl_{11}]$ part will reorganize in an

ultrafast time and the excitons will transfer to triplet state (3P) through ISC process, and the strong SR in ES leads to the large Stokes shift. At sufficiently low temperature, the triplet state can transit to the ground state (GS) through radiative combination with few thermal-assisted nonradiative combinations, which result in ultra-high PLQY. As the temperature rises, the nonradiative pathway will increase significantly with the assistance of heat, which will cause inevitable reduction in PLQY. Br-based compound is more temperature-sensitive and is easier to de-trapping to the GS through the phonon absorption-induced nonradiative recombination and show low PLQY at RT (Figure 5a). When replacing Br^- anions by Cl^- anions, the enhanced e–p interaction and the weakened thermal-assisted nonradiative recombination resulting in the enhanced PLQY (Figure 5b). Finally, the highest PLQY will be obtained when Cl^- completely replace Br^- (Figure 5c). Simultaneously, the PL spectra exhibits an obvious blue shift as the higher excited state energy for Cl structures, in that case, we both achieved PL spectral shift and enhancement in PLQY by such halogen replacement.

3. Conclusion

In summary, we obtained OD mixed halogen multicomponent metal halides single crystals of $(C_9NH_{20})_9Pb_3Zn_2Br_{19(1-x)}Cl_{19x}$ ($x = 0-1$). Tunable emissions along with variable PLQYs were obtained in this series of solid solutions, and the competitive substitution of the bromine to chlorine was found, as formed firstly in $[ZnBr_{4-x}Cl_x]^{2-}$ tetrahedron and then in the $[Pb_3Br_{11-x}Cl_x]^{5-}$ trimer. Optical analysis and DFT calculations revealed that the tunable emissions from yellow to green originated from STEs emission of $[Pb_3(Br/Cl)_{11}]^{5-}$ clusters in different chemical environment. Moreover, the introduction of Cl^- ions both enhance the e–p coupling and inhibit the thermal-assisted nonradiative recombination, which result in a significantly emission enhancement as verified by the theoretical calculations. Our work uncovered the role of halogen ions in photophysical processes and proposed a feasible way to improve the PL properties in OD hybrids, which will promote the development of high-performance new materials in OD fields.

Experimental Section

Synthesis: Zinc (II) bromide (99.9%), zinc (II) chloride (99.99%), lead bromide (99%), lead chloride (99.99%), 1-butyl-1-methylpyrrolidinium bromide ($C_9NH_{20}Br$) (99%), 1-butyl-1-methylpyrrolidinium chloride ($C_9NH_{20}Cl$) (99%), and *N,N*-dimethylformamide (DMF) (99.9%) were purchased from Aladdin Co. Ltd. (Shanghai, China). $(C_9NH_{20})_9Pb_3Zn_2Br_{19(1-x)}Cl_{19x}$ ($x = 0, 0.2, 0.4, 0.6, 0.8, \text{ and } 1$) single crystals were synthesized as follows: 4.5 mmol of $C_9NH_{20}Br/C_9NH_{20}Cl$, 1.0 mmol of $ZnBr_2/ZnCl_2$, and 1.5 mmol of $PbBr_2/PbCl_2$ were dissolved in 1.5 mL of DMF under heating and continuous stirring at 323 K. Colorless crystals were obtained by slowly cooling the saturated solution to RT with the controlled cooling rate to obtain the crystals with different sizes.

Characterization: The diffraction patterns were collected from single crystals of $(C_9NH_{20})_9[Pb_3Br_{11}](ZnBr_4)_2$ and $(C_9NH_{20})_9[Pb_3Cl_{11}](ZnCl_4)_2$ at 296 K using the SMART APEX II X-ray single crystal diffractometers (Bruker AXS, analytical equipment of Krasnoyarsk Center of collective use

of SB RAS) equipped with a CCD detector, graphite monochromator, and Mo $K\alpha$ radiation source. The absorption corrections were applied using the SADABS program. The structures were solved by the direct methods using SHELXS and refined using the SHELXL program.^[15] All hydrogen atoms were linked with C,N atoms and positioned geometrically as riding on their parent atoms with $U_{iso}(H) = U_{eq}(C,N)$. Powder X-ray diffraction (PXRD) data of $(C_9NH_{20})_9Pb_3Zn_2Br_{19(1-x)}Cl_{19x}$ ($x = 0-1$) were obtained using diffractometer D8 ADVANCE (Bruker) equipped by a VANTEC detector with a Ni filter. The measurements were made using Cu $K\alpha$ radiation. The structural parameters defined by single crystal analysis were used as a basic in powder pattern Rietveld refinement. The refinement was produced using TOPAS 4.2 software.^[16] TGA was performed on a Setaram Labsys Evo at $10\text{ }^\circ\text{C min}^{-1}$ in an argon flow from RT to $800\text{ }^\circ\text{C}$. The photoluminescence excitation (PLE) and emission (PL) spectra at RT were recorded by an Edinburgh FLS920 fluorescence spectrophotometer with the Xe900 lamp as the excitation source. For low-temperature measurements, sample was cooled in a liquid nitrogen cryostat on Oxford Instruments that was attached to the FLS920. The PLQY of title samples was measured using the integrated sphere on the same FLS920 instrument, and white $BaSO_4$ powder was used as a reference to measure the absorption. The luminescence decay curves were obtained by the FLS920 using an nF900 and μ F900 flash lamp and as the excitation source. The diffuse reflection spectra were measured on a UV-Vis-NIR spectrophotometer (SHIMADZU UV-3600) supplied with an integrating sphere. The power-dependent PL spectra were measured using the 375 nm (LE-LS-375-140TFCA, 1–140 mW) laser. Femtosecond transient (fs-TA) absorption experiments were performed by using a self-made femtosecond pump-probe setup, and the details can be also found in other references.^[17] Laser pulses (800 nm, 50 fs pulse length, 1 kHz repetition rate) were generated by a Ti:sapphire femtosecond laser (Hurricane, Spectra-Physics) source. An optical parametric amplifier was used to change the laser wavelength. For the probe beam, we use a white light continuum (WLC) generated by a 2 mm thick CaF_2 with window from 350 to 800 nm. The sample was excited by 367 nm laser pulse.

Computational Methods: Calculations were performed within the framework of the density functional theory by using plane-wave pseudopotentials as implemented in the Vienna Ab initio Simulation Package.^[18] The electron-ion interactions were described by the projected augmented wave (PAW) pseudopotentials^[19] with the 6s and 6p (Pb), 4s and 4p (Br), 2s and 2p (N), 2s and 2p (C), 4d and 4p (Zn), and 1s (H) electrons treated explicitly as valence electrons. We employed the generalized gradient approximation formulated by Perdew, Burke, and Ernzerhof as the exchange correlation functional.²⁵ Structural optimizations were done with the kinetic-energy cutoff of 500 eV and the electronic Brillouin zone k-point of the Γ point, which ensures residual forces smaller than $0.05\text{ eV } \text{Å}^{-1}$.

Supporting Information

Supporting Information is available from the Wiley Online Library or from the author.

Acknowledgements

M.L., Y.L. contributed equally to this work. This work was supported by the National Natural Science Foundation of China (51961145101, 51972118, and 51722202), Fundamental Research Funds for the Central Universities (FRFTP-18-002C1), the Guangdong Provincial Science & Technology Project (2018A050506004), and the Local Innovative and Research Teams Project of Guangdong Pearl River Talents Program (2017BT01 \times 137). This work was also funded by RFBR according to the research project No. 19-52-80003. The work at Jilin University is supported by the National Natural Science Foundation of China (Grant No. 61722403 and 11674121) and Jilin Province Science and Technology Development Program (Grant No. 20190201016J). Calculations were performed in part at the high performance computing center of Jilin University.

Conflict of Interest

The authors declare no conflict of interest.

Keywords

halogen substitution, hybrid metal halides, photoluminescence quantum yield

Received: March 10, 2020

Published online:

- [1] J. K. Pious, A. Katre, C. Muthu, S. Chakraborty, S. Krishna, V. C. Nair, *Chem. Mater.* **2019**, *31*, 1941.
- [2] a) M. Worku, Y. Tian, C. K. Zhou, S. Lee, Q. Meisner, Y. Zhou, B. W. Ma, *ACS Appl. Mater. Interfaces* **2018**, *10*, 30051; b) M. Z. Li, J. Zhou, G. J. Zhou, M. S. Molokeev, J. Zhao, V. Morad, M. V. Kovalenko, Z. G. Xia, *Angew. Chem., Int. Ed.* **2019**, *58*, 18670.
- [3] V. Morad, Y. Shynkarenko, S. Yakunin, A. Brumberg, R. D. Schaller, M. V. Kovalenko, *J. Am. Chem. Soc.* **2019**, *141*, 9764.
- [4] a) C. L. Jiang, N. Zhong, C. H. Luo, H. C. Lin, Y. Y. Zhang, H. Peng, C. G. Duan, *Chem. Commun.* **2017**, *53*, 5954; b) M. Z. Li, J. Zhou, M. S. Molokeev, X. X. Jiang, Z. S. Lin, J. Zhao, Z. G. Xia, *Inorg. Chem.* **2019**, *58*, 13464.
- [5] a) J. Zhou, M. Z. Li, L. X. Ning, R. L. Zhang, M. S. Molokeev, J. Zhao, S. Q. Yang, K. L. Han, Z. G. Xia, *J. Phys. Chem. Lett.* **2019**, *10*, 1337; b) Z. Y. Li, Y. Li, P. Liang, T. L. Zhou, T. L. Wang, R. J. Xie, *Chem. Mater.* **2019**, *31*, 9363; c) C. K. Zhou, H. R. Lin, M. Worku, J. Neu, Y. Zhou, Y. Tian, S. Lee, P. Djurovich, T. Siegrist, B. W. Ma, *J. Am. Chem. Soc.* **2018**, *140*, 13181; d) C. K. Zhou, H. R. Lin, J. Neu, Y. Zhou, M. Chaaban, S. Lee, M. Worku, B. H. Chen, R. Clark, W. H. Cheng, J. J. Guan, P. Djurovich, D. Z. Zhang, X. J. Lü, J. Bullock, C. Pak, M. Shatruk, M. H. Du, T. Siegrist, B. W. Ma, *ACS Energy Lett.* **2019**, *4*, 1579.
- [6] a) L. K. Gong, J. R. Li, Z. F. Wu, B. Hu, Z. P. Wang, N. N. Shen, Q. Q. Hu, Z. H. Deng, Z. Z. Zhang, J. J. Fu, K. Z. Du, X. Y. Huang, *J. Mater. Chem. C* **2019**, *7*, 9803; b) B. B. Cui, Y. Han, B. L. Huang, Y. Z. Zhao, X. X. Wu, L. Liu, G. Y. Cao, Q. Du, N. Liu, W. Zou, M. Z. Sun, L. Wang, X. F. Liu, J. P. Wang, H. P. Zhou, Q. Chen, *Nat. Commun.* **2019**, *10*, 5190.
- [7] a) M. D. Smith, B. A. Connor, H. I. Karunadasa, *Chem. Rev.* **2019**, *119*, 3104; b) L. L. Mao, Y. L. Wu, C. C. Stoumpos, B. Traore, C. Katan, J. Even, M. R. Wasielewski, M. G. Kanatzidis, *J. Am. Chem. Soc.* **2017**, *139*, 11956; c) D. W. Yang, J. Lv, X. G. Zhao, Q. L. Xu, Y. H. Fu, Y. Q. Zhan, A. Zunger, L. J. Zhang, *Chem. Mater.* **2017**, *29*, 524.
- [8] a) X. T. Li, P. J. Guo, M. Kepenekian, I. Hadar, C. Katan, J. Even, C. C. Stoumpos, R. D. Schaller, M. G. Kanatzidis, *Chem. Mater.* **2019**, *31*, 3582; b) R. Gautier, M. Paris, F. Massuyeau, *J. Am. Chem. Soc.* **2019**, *141*, 12619.
- [9] a) T. Hu, M. D. Smith, E. R. Dohner, M. J. Sher, X. Wu, M. T. Trinh, A. Fisher, J. Corbett, X. Y. Zhu, H. I. Karunadasa, A. M. Lindenberg, *J. Phys. Chem. Lett.* **2016**, *7*, 2258; b) K. Thirumal, W. K. Chong, W. Xie, R. Ganguly, S. K. Muduli, M. Sherburne, M. Asta, S. Mhaisalkar, T. C. Sum, H. S. Soo, N. Mathews, *Chem. Mater.* **2017**, *29*, 3947. c) H. L. Shi, D. Han, S. Y. Chen, M. H. Du, *Phys. Rev. Mater.* **2019**, *3*, 034604.
- [10] S. Yakunin, B. M. Benin, Y. Shynkarenko, O. Nazarenko, M. I. Bodnarchuk, D. N. Dirin, C. Hofer, S. Cattaneo, M. V. Kovalenko, *Nat. Mater.* **2019**, *18*, 846.

- [11] a) K. M. McCall, C. C. Stoumpos, S. S. Kostina, M. G. Kanatzidis, B. W. Wessels, *Chem. Mater.* **2017**, 29, 4129; b) P. W. M. Jacobs, *J. Phys. Chem. Solids* **1991**, 52, 35.
- [12] a) M. Iwanaga, M. Watanabe, T. Hayashi, *Phys. Rev. B* **2000**, 62, 10766; b) M. Iwanaga, M. Shirai, K. Tanaka, T. Hayashi, *Phys. Rev. B* **2002**, 66, 4304.
- [13] M. A. Baldo, D. F. O'Brien, Y. You, A. Shoustikov, S. Sibley, M. E. Thompson, S. R. Forrest, *Nature* **1998**, 395, 151.
- [14] M. D. Smith, H. I. Karunadasa, *Acc. Chem. Res.* **2018**, 51, 619.
- [15] Sheldrick, G. M. , *Acta Crystallogr., Sect. A: Found. Crystallogr.* **2008**, 64, 112.
- [16] V. TOPAS, Bruker AXS, Karlsruhe, Germany **2008**.
- [17] a) S. Q. Yang, Y. Zhang, K. L. Han, *J. Lumin.* **2019**, 206, 46; b) S. Q. Yang, K. L. Han, *J. Phys. Chem. A* **2016**, 120, 4961.
- [18] a) M. C. Payne, M. P. Teter, D. C. Allan, T. A. Arias, J. D. Joannopoulos, *Rev. Mod. Phys.* **1992**, 64, 1045. b) G. Kresse, *Phys. Rev. B* **1996**, 54, 11169.
- [19] G. Kresse, D. Joubert, *Phys. Rev. B* **1999**, 59, 1758.